

Directional spatial structure of dissociated elongated molecular condensates

Magnus Ögren,¹ C. M. Savage,² and K. V. Kheruntsyan¹

¹*ARC Centre of Excellence for Quantum-Atom Optics, School of Physical Sciences,
University of Queensland, Brisbane, QLD 4072, Australia*

²*ARC Centre of Excellence for Quantum-Atom Optics, Department of Physics,
Australian National University, Canberra ACT 0200, Australia*

(Dated: October 31, 2018)

Ultra-cold clouds of dimeric molecules can dissociate into quantum mechanically correlated constituent atoms that are either bosons or fermions. We theoretically model the dissociation of cigar shaped molecular condensates, for which this difference manifests as complementary geometric structures of the dissociated atoms. For atomic bosons beams form along the long axis of the molecular condensate. For atomic fermions beams form along the short axis. This directional beaming simplifies the measurement of correlations between the atoms through relative number squeezing.

PACS numbers: 03.75.-b, 03.65.-w, 05.30.-d, 33.80.Gj

The difference between bosons and fermions is fundamental in physics. Ultra-cold degenerate quantum gases enable new kinds of explorations and applications of this difference. For example in Hanbury Brown and Twiss type measurements bosonic ⁴He atoms are observed to be bunched while fermionic ³He atoms are anti-bunched [1]. Besides such local spatial correlations, non-local correlations between pairs of atoms with opposite momenta have also been observed for both fermionic atoms [2] and bosonic atoms [3]. Such atom pairs, generated by dissociation of molecular-dimers [2], or by four-wave mixing [3], are predicted to be entangled [4, 5, 6, 7, 8, 9, 10, 11]. However the existence of non-classical Einstein-Podolsky-Rosen type correlations [4, 8] between atom pairs in these systems remains to be experimentally confirmed.

We report an analysis of the effect of particle statistics on the dissociation of highly anisotropic Bose-Einstein condensates (BECs) of molecular dimers. When the dissociated atoms are bosons we confirm the expected beaming of atoms along the long axis of the cigar shaped molecular condensate by stimulated emission [7]. However, when the atoms are fermions we find an unexpected beaming in the orthogonal direction, i.e., along the short condensate axis. The effect is due to Pauli blocking followed by atom-atom recombination which reduces the atomic density along the long axis. We also find enhanced relative number squeezing between the atoms in the half-spaces occupied by the oppositely directed beams.

Directionality effects due to bosonic amplification have been observed [12, 13] in superradiant light scattering from elongated condensates [7, 14, 15]. The fermionic counterpart of the effect due to Pauli blocking has not been discussed before to the best of our knowledge.

The effective quantum field theory Hamiltonian describing the system is given, in a rotating frame, by [16]

$$\hat{H} = \hat{H}_0 + \hbar \int d\mathbf{x} \left[\sum_{i=1,2} \Delta \hat{\Psi}_i^\dagger \hat{\Psi}_i - ig(\mathbf{x}) \left(\hat{\Psi}_1 \hat{\Psi}_2 - \hat{\Psi}_2^\dagger \hat{\Psi}_1^\dagger \right) \right]. \quad (1)$$

Here, $\hat{\Psi}_i(\mathbf{x}, t)$ ($i = 1, 2$) are the field operators for the atoms, which are two different spin states of the same isotope of mass m , and may be either bosonic or fermionic. The field operators satisfy the respective commutation or anti-commutation relations, $[\hat{\Psi}_i(\mathbf{x}, t), \hat{\Psi}_j^\dagger(\mathbf{x}', t)] = \delta_{ij} \delta^2(\mathbf{x} - \mathbf{x}')$ and $\{\hat{\Psi}_i(\mathbf{x}, t), \hat{\Psi}_j^\dagger(\mathbf{x}', t)\} = \delta_{ij} \delta^2(\mathbf{x} - \mathbf{x}')$. In the following we shall only consider two spatial dimensions, with $\mathbf{x} = (x, y)$. However we expect our results to be at least qualitatively valid for three-dimensional systems.

The first term in Eq. (1) describes the kinetic energy of the atoms $\hat{H}_0 = \int d\mathbf{x} \sum_{i=1,2} \hbar^2 |\nabla \hat{\Psi}_i|^2 / 2m$. The detuning Δ is defined so that spontaneous dissociation of molecules corresponds to $\Delta < 0$, with $2\hbar|\Delta|$ being the total dissociation energy that is converted into the kinetic energy of atom pairs [17, 18]. For molecules at rest, the dissociation primarily populates the resonant atomic modes in the two spin states having equal but opposite momenta, $\hbar\mathbf{k}_1 = -\hbar\mathbf{k}_2$, with the absolute wavenumber equal to $k_0 = |\mathbf{k}_1| = |\mathbf{k}_2| = \sqrt{2m|\Delta|/\hbar}$.

In our analysis we use the undepleted molecular field approximation. It is valid for short dissociation times during which the converted fraction of molecules does not exceed about 10% [17, 19]. In the regime of validity of the undepleted molecular approximation, the dissociation typically produces low density atomic clouds for which the s -wave scattering interactions are negligible [19]; hence their absence from our Hamiltonian. Additionally, the atom-molecule interactions can be neglected if the respective interaction energy per atom is much smaller than the total dissociation energy $2\hbar|\Delta|$. We have confirmed the validity of our approximations (which improve with increasing $|\Delta|$) in the case of dissociation into bosonic atoms by comparing the present results with exact, first-principles simulations using the positive- P representation [19]. For the case of fermionic atoms, first-principles simulations with multimode inhomogeneous molecular condensates remain under development [20], and such a comparison is not presently possi-

ble.

We assume that the bosonic molecules are in a coherent state initially, with the density profile $\rho_M(\mathbf{x})$ given by the ground state solution of the Gross-Pitaevskii equation with an anisotropic harmonic trap. We then have an effective, spatially dependent coupling

$$g(\mathbf{x}) = \chi \sqrt{\rho_M(\mathbf{x})}. \quad (2)$$

The coupling coefficient χ [17] is responsible for coherent conversion of molecules into atom pairs, e.g. via optical Raman transitions, an rf pulse, or a Feshbach resonance sweep [21, 22, 23, 24, 25]. We assume that once the dissociation is switched on at time $t = 0$, the trapping potential is switched off, so that the evolution is taking place in free space. Thus the role of the trapping potential is reduced to defining the initial shape of the molecular BEC.

The Heisenberg equations for the atomic fields in the Hamiltonian (1) are then:

$$\begin{aligned} \frac{\partial \widehat{\Psi}_1(\mathbf{x}, t)}{\partial t} &= i \left[\frac{\hbar}{2m} \nabla^2 - \Delta \right] \widehat{\Psi}_1(\mathbf{x}, t) \pm g(\mathbf{x}) \widehat{\Psi}_2^\dagger(\mathbf{x}, t), \\ \frac{\partial \widehat{\Psi}_2^\dagger(\mathbf{x}, t)}{\partial t} &= -i \left[\frac{\hbar}{2m} \nabla^2 - \Delta \right] \widehat{\Psi}_2^\dagger(\mathbf{x}, t) + g(\mathbf{x}) \widehat{\Psi}_1(\mathbf{x}, t). \end{aligned} \quad (3)$$

The $+/-$ in the first equation correspond to bosonic/fermionic atoms.

Expanding in plane wave modes, $\widehat{\Psi}_j(\mathbf{x}, t) = \int d^2\mathbf{k} \widehat{a}_j(\mathbf{k}, t) \exp(-i\mathbf{k} \cdot \mathbf{x})/2\pi$, where the operator amplitudes satisfy commutation or anticommutation relations, $[\widehat{a}_i(\mathbf{k}, t), \widehat{a}_j^\dagger(\mathbf{k}', t)] = \delta_{ij} \delta^2(\mathbf{k} - \mathbf{k}')$ or $\{\widehat{a}_i(\mathbf{k}, t), \widehat{a}_j^\dagger(\mathbf{k}', t)\} = \delta_{ij} \delta^2(\mathbf{k} - \mathbf{k}')$, according to the underlying statistics. The partial differential equations (3) reduce to a set of linear ordinary differential equations,

$$\begin{aligned} \frac{d\widehat{a}_1(\mathbf{k}, t)}{dt} &= -i\Delta_k \widehat{a}_1(\mathbf{k}, t) \pm \int \frac{d^2\mathbf{q}}{2\pi} \widetilde{g}(\mathbf{q} + \mathbf{k}) \widehat{a}_2^\dagger(\mathbf{q}, t), \\ \frac{d\widehat{a}_2^\dagger(\mathbf{k}, t)}{dt} &= i\Delta_k \widehat{a}_2^\dagger(\mathbf{k}, t) + \int \frac{d^2\mathbf{q}}{2\pi} \widetilde{g}(\mathbf{q} - \mathbf{k}) \widehat{a}_1(-\mathbf{q}, t), \end{aligned} \quad (4)$$

where $\widetilde{g}(\mathbf{k}) = \int d^2\mathbf{x} g(\mathbf{x}) \exp(i\mathbf{k} \cdot \mathbf{x})/2\pi$ is the Fourier transform of $g(\mathbf{x})$ and $\Delta_k \equiv \hbar k^2/(2m) + \Delta$, where $k = |\mathbf{k}|$. For vacuum initial conditions the non-zero second-order moments are the normal and anomalous densities; $n_i(\mathbf{k}, \mathbf{k}', t) \equiv \langle \widehat{a}_i^\dagger(\mathbf{k}, t) \widehat{a}_i(\mathbf{k}', t) \rangle$ and $m_{12}(\mathbf{k}, \mathbf{k}', t) \equiv \langle \widehat{a}_1(\mathbf{k}, t) \widehat{a}_2(\mathbf{k}', t) \rangle$. Higher-order moments can be obtained from these second-order moments using Wick's theorem, as the Hamiltonian is quadratic in the field operators in the undepleted molecular approximation.

In a finite quantization volume the wave-vector \mathbf{k} is discrete and the plane wave mode annihilation and creation operators may be organized into a vector \vec{a} . The Heisenberg equations (4) may then be written in vector-matrix form as $d\vec{a}/dt = M\vec{a}$, where M is a matrix of

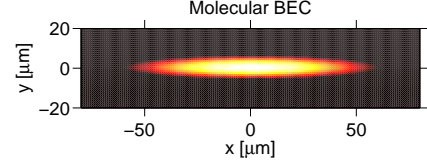


Figure 1: (color online) Density in position space for the initial molecular condensate. It corresponds to the ground state of a harmonic trap with TF radii: $R_{TF,x} \simeq 60 \mu\text{m}$ and $R_{TF,y} \simeq 6 \mu\text{m}$.

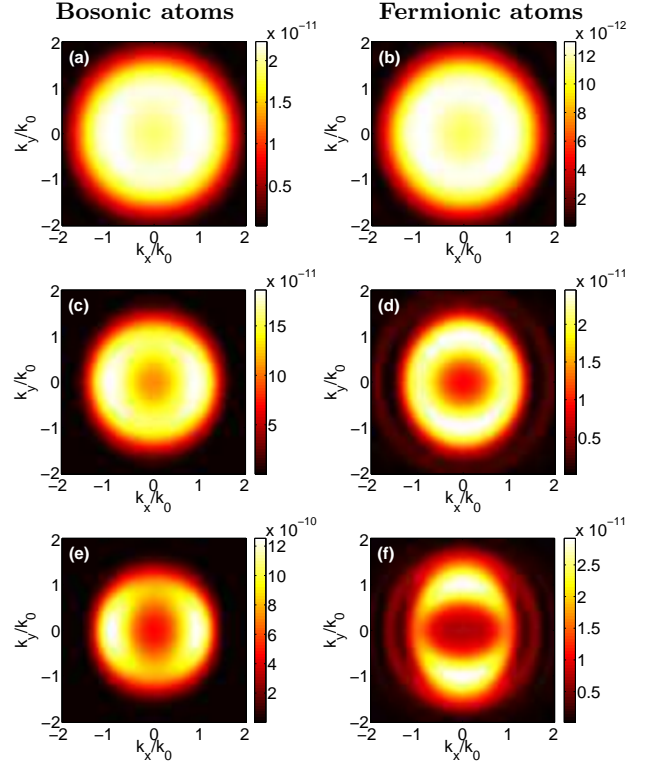


Figure 2: (color online) Atomic density in momentum space (in units of m^2) at different times t after the start of dissociation. The left and right columns are for bosonic and fermionic atoms, respectively. We have chosen the times $t_1/t_0 = 1.1$ for (a) and (b), $t_2/t_0 = 2.2$ for (c) and (d), and $t_3/t_0 = 3.3$ for (e) and (f). Here $t_0 = 1/(\chi\sqrt{\rho_{M,0}}) = 2.5 \text{ ms}$ is the time scale.

complex numbers. Linearity ensures that the solutions of these operator equations can be found by numerically computing the matrix exponential $\exp(Mt)$. We used an 81×81 numerical lattice in momentum space, which gave the same results as for a 61×61 lattice.

Here we explore the role of a strongly anisotropic system by assuming that the initial molecular condensate was trapped in a harmonic potential with a frequency along the y axis ω_y that is ten times that along the x axis; $\omega_y = 10\omega_x$. We assume a molecule-molecule scattering length such that the Thomas-Fermi (TF) approximation is valid. The corresponding molecular density profile is $\rho_M = \rho_{M,0} (1 - x^2/R_{TF,x}^2 - y^2/R_{TF,y}^2)$, where the $R_{TF,i}$

are the TF-radii in each direction. The parameter values we used are given in Ref. [26].

Fig. 5 shows the density of our initial two-dimensional molecular condensate in position space. Fig. 2 shows the total density of the dissociated atoms in momentum space, at three times as dissociation progresses. The left column shows bosonic atoms, and the right column shows fermionic atoms. Note that after sufficient time-of-flight expansion, these momentum space distributions are reproduced in position space [2, 10]. At the earliest time there is little difference between the bosons and fermions, and the width of the distribution is determined by the energy-time uncertainty relation. Later, the spatial distributions of the bosons and fermions develop quite differently. For bosons, our results can be compared with first-principles simulations using the positive- P representation [19], in which the molecular field and its depletion is treated quantum mechanically; the comparison is given in Ref. [27] and shows good agreement.

The highest densities of bosons develop along the long axis of the molecular condensate. This is due to Bose stimulation, which in the undepleted molecular field approximation leads to approximately exponential growth of the atom number. In contrast, the highest densities of fermions occur in the orthogonal direction; that is along the short axis of the initial molecular condensate. Physically, the effect is due to Pauli blocking followed by the reduction of the atomic density due to atom-atom recombination along the long axis. The dynamics along the short axis (for sufficiently small $R_{\text{TF},y}$), on the other hand, does not reach the regime dominated by saturation of mode populations and atom-atom recombination as the atoms propagating along y leave the molecular condensate earlier than those propagating along x .

Mathematically, the difference is due to the sign difference on the right-hand-side of the Heisenberg equations (3), corresponding to bosons and fermions. As noted in Ref. [28] the sign difference determines $\sinh(\alpha_k \tau)$ population growth for bosons, and $\sin(\alpha_k \tau)$ population oscillations for fermions; where $\tau = t/t_0$ is a dimensionless time, with $t_0 = 1/(\chi\sqrt{\rho_{\text{M},0}})$, and $\alpha_k = \sqrt{1 \pm t_0^2(\hbar k^2/(2m) + \Delta)^2}$; here, the + corresponding to fermions and the - to bosons.

The fermionic oscillations – both in momentum space and in time – can be seen in Figs. 2 (d) and (f) and in Fig. 3. As the solutions of Ref. [28] are for spatially homogenous systems they do not quantitatively describe these minima for our inhomogeneous molecular condensate. Nevertheless they predict aspects of the qualitative behavior, such as the movement of the density minima and maxima to lower values of k_x with increasing time; Figs. 2 (d) and (f). The single density maximum along the k_y axis is a result of the small TF radius along that axis, $R_{\text{TF},y} = 6 \mu\text{m}$. The atomic velocity at $|k/k_0| = 1$ is 0.95 mm s^{-1} , so during $t_1 = 1.1t_0 = 1.1(2.5 \text{ ms})$ the

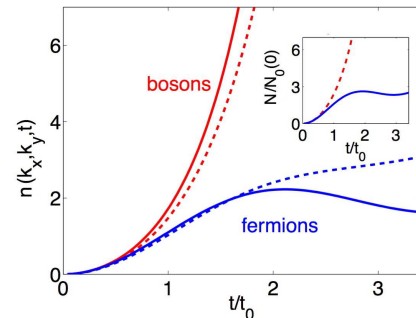


Figure 3: (color online) Atomic density in momentum space at the position of resonance ($|\mathbf{k}| = k_0$) along the two different Cartesian directions, in units of 10^{-11} m^2 . The two upper (red) curves are for bosons which grow exponentially due to Bose stimulation. The two lower (blue) curves are for fermions. Solid lines are along the k_x -direction ($k_x = k_0, k_y = 0$), dashed lines are along the k_y -direction ($k_x = 0, k_y = k_0$). The inset shows the fractional atom number (relative to the total initial number of molecules), in units of tenths of a percent, for fermions (solid blue) and bosons (dashed red).

atoms travel $2.6 \mu\text{m}$, and during $t_3 = 3.3t_0$ they travel $7.8 \mu\text{m}$, which is greater than the TF radius $R_{\text{TF},y}$. Hence a particular atom traveling in the y direction typically interacts with the molecular condensate for less than the time t_3 . This accounts for the similarity of Figs. 2 (d) and (f) along the y axis.

We have used our solutions of the Heisenberg equations (4) to calculate the correlations between atom number fluctuations in the two different spin states 1 and 2. We considered momentum areas centered on the opposite resonant momenta, $\hbar\mathbf{k}_0$ and $-\hbar\mathbf{k}_0$, for the smallest and largest possible areas in which the atoms are captured and their number is measured. The smallest momentum areas are the numerical lattice areas, and the largest are opposite halves of the momentum space. These are orientated differently for fermions and bosons, guided by Figs. 2 (e) and (f), to capture one beam in each half: for bosons the halves are split by the k_y axis and for fermions by the k_x axis.

For the case of the smallest momentum area (the area of the numerical lattice cell, $\Delta k_x \Delta k_y$), we define the atom number operators via $\hat{n}_{j,\pm\mathbf{k}_0}(t) = \hat{n}_j(\pm\mathbf{k}_0, t) \Delta k_x \Delta k_y$, where $\mathbf{k}_0 = k_0 \mathbf{e}_x$ for bosons and $\mathbf{k}_0 = k_0 \mathbf{e}_y$ for fermions, with \mathbf{e}_x and \mathbf{e}_y being the Cartesian unit vectors. We quantify the correlations by the normalized relative atom number variance,

$$V_{\mathbf{k}_0, -\mathbf{k}_0}(t) = \langle [\Delta(\hat{n}_{1,\mathbf{k}_0} - \hat{n}_{2,-\mathbf{k}_0})]^2 \rangle / \Delta_{\text{SN}}, \quad (5)$$

where $\Delta\hat{C} = \hat{C} - \langle\hat{C}\rangle$ is the fluctuation in \hat{C} and $\Delta_{\text{SN}} = \langle(\Delta\hat{n}_{1,\mathbf{k}_0})^2\rangle + \langle(\Delta\hat{n}_{2,-\mathbf{k}_0})^2\rangle$ defines the uncorrelated shot-noise level. Variance $V_{\mathbf{k}_0, -\mathbf{k}_0}(t) < 1$ implies squeezing of the relative number fluctuations below the shot-noise level. The results (see Ref. [27] for details) are shown

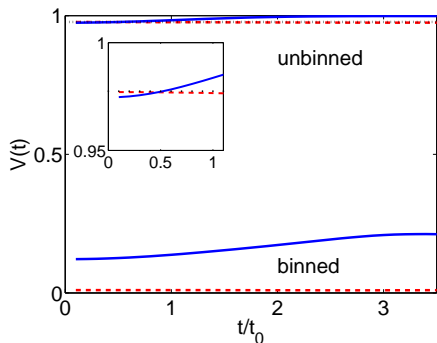


Figure 4: (color online) Relative number variance according to Eqs. (5) and (6), raw (unbinned) and binned, for fermions (solid blue) and bosons (dashed red). The dotted (black) line in the inset is the $t \ll t_0$ asymptote, Eq. (7).

in Fig. 4 (upper curves), where we see relatively small degree of squeezing for this “raw” (unbinned) case.

The squeezing in the relative number can be enhanced for larger counting areas, which we refer to as binning [10]. For the largest pair of bins coinciding with the left (L) and right (R) halves of the momentum space for bosons, and with the bottom (B) and top (T) halves for fermions, we can introduce particle number operators $\hat{N}_i^{\text{L(R)}}$ and $\hat{N}_i^{\text{B(T)}}$ ($i = 1, 2$). The normalized variance of the relative number fluctuations between the spin states 1 and 2 is defined similarly to Eq. (5),

$$V_{\text{LR(BT)}}(t) = \langle [\Delta(\hat{N}_1^{\text{R(T)}}) - \hat{N}_2^{\text{L(B)}}]^2 \rangle / \Delta_{\text{SN}}. \quad (6)$$

The results for $V_{\text{LR(BT)}}(t)$ (see Ref. [27] for details) are shown in Fig. 4; comparing the upper and lower curves, we see that binning into momentum half-spaces reduces the relative number variance, or increases the degree of squeezing, by a factor of about ten for fermions and a hundred for bosons. This difference is due to the different momentum uncertainties along the long and short spatial axes. The momentum uncertainty is about ten times smaller along the long axis, which is the bosonic beaming direction. Hence there are about ten times less correlated pairs ending up in the same momentum half-space. For the fermions, on the other hand, the relatively high momentum uncertainty in the beaming direction produces more pairs in the same half-space, reducing the number difference squeezing.

In the case of unbinned atom numbers the fermionic and bosonic cases have a common short time asymptote that can be determined analytically using a perturbative approach [29]. Applying it to our 2D system gives

$$V_{\mathbf{k}_0, -\mathbf{k}_0} = 1 - 2R_{TF,x}R_{TF,y}\Delta k_x\Delta k_y/(9\pi) \simeq 0.978, \quad (7)$$

which agrees with our numerical results (see Fig. 4).

In summary, we have shown that dissociation of elongated condensates of molecular dimers into atoms can

produce qualitatively different geometrical distributions for bosonic and fermionic atoms. These are in the form of “twin” beams in opposite half-spaces. The squeezing of the relative atom number fluctuations between these beams can be quite strong.

The authors acknowledge support from the Australian Research Council through the ARC Centre of Excellence scheme. MÖ acknowledges IPRS/UQILAS.

-
- [1] T. Jelte *et al.*, Nature (London) **445**, 402 (2007).
 - [2] M. Greiner *et al.*, Phys. Rev. Lett. **94**, 110401 (2005).
 - [3] A. Perrin *et al.*, Phys. Rev. Lett. **99**, 150405 (2007).
 - [4] H. Pu and P. Meystre, Phys. Rev. Lett. **85**, 3987 (2000); L.-M. Duan *et al.*, Nature (London) **409**, 63 (2001).
 - [5] V. A. Yurovsky, Phys. Rev. A **65**, 033605 (2002).
 - [6] K. V. Kheruntsyan and P. D. Drummond, Phys. Rev. A **66**, 031602(R) (2002).
 - [7] A. Vardi and M. G. Moore, Phys. Rev. Lett. **89**, 090403 (2002).
 - [8] K. V. Kheruntsyan, M. K. Olsen, and P. D. Drummond, Phys. Rev. Lett. **95**, 150405 (2005).
 - [9] B. Zhao *et al.*, Phys. Rev. A **75**, 042312 (2007).
 - [10] C. M. Savage and K. V. Kheruntsyan, Phys. Rev. Lett. **99**, 220404 (2007).
 - [11] A. Perrin *et al.*, New J. Physics **10**, 045021 (2008).
 - [12] S. Inouye *et al.*, Science **285**, 571 (1999).
 - [13] M. Kozuma *et al.*, Science **286**, 2309 (1999).
 - [14] M. G. Moore and P. Meystre, Phys. Rev. Lett. **83**, 5202 (1999).
 - [15] H. Uys and P. Meystre, Phys. Rev. A **77**, 063614 (2008).
 - [16] K. V. Kheruntsyan and P. D. Drummond, Phys. Rev. A **61**, 063816 (2000).
 - [17] M. J. Davis *et al.*, Phys. Rev. A **77**, 023617 (2008).
 - [18] M. W. Jack and H. Pu, Phys. Rev. A **72**, 063625 (2005).
 - [19] C. M. Savage, P. E. Schwenn, and K. V. Kheruntsyan, Phys. Rev. A **74**, 033620 (2006).
 - [20] J. F. Corney and P. D. Drummond, Phys. Rev. Lett. **93**, 260401 (2004); Phys. Rev. B **73**, 125112 (2006).
 - [21] P. D. Drummond, K. V. Kheruntsyan, and H. He, Phys. Rev. Lett. **81**, 3055 (1998); D. J. Heinzen *et al.*, *ibid.* **84**, 5029 (2000).
 - [22] E. Timmermans *et al.*, Phys. Rep. **315**, 199 (1999); J. Javanainen and M. Mackie, Phys. Rev. A **59**, R3186 (1999).
 - [23] S. J. Kokkelmans *et al.*, Phys. Rev. A **65**, 053617 (2002).
 - [24] P. D. Drummond and K. V. Kheruntsyan, Phys. Rev. A **70**, 033609 (2004).
 - [25] R. A. Duine and H. T. C. Stoof, Phys. Rep. **86**, 115 (2004); T. Köhler, K. Góral, and P. S. Julienne, Rev. Mod. Phys. **78**, 1311 (2006).
 - [26] Molecular peak density $\rho_{M,0} = 3.2 \times 10^{13} \text{ m}^{-2}$; number of molecules $N_M = 2 \times 10^4$; atomic mass $m = 6.5 \times 10^{-26} \text{ kg}$ (^{40}K); molecule-atom coupling strength $\chi = 7.1 \times 10^{-5} \text{ ms}^{-1}$; and dissociation detuning $\Delta = -281 \text{ s}^{-1}$, which is large enough to ensure that the dissociation energy is larger than thermal at nK temperatures. The momentum lattice had a spacing $\Delta k_x = \Delta k_y = 3.0 \times 10^4 \text{ m}^{-1}$, which is smaller than the smallest width of the molecular momentum distribution.
 - [27] See EPAPS Document No. E-PRLTAO-XXX-XXXXXX

at <http://www.aip.org/pubservs/epaps.html>.

- [28] K. V. Kheruntsyan, Phys. Rev. Lett. **96**, 110401 (2006).
 [29] M. Ögren and K. V. Kheruntsyan, Phys. Rev. A **78**, 011602(R) (2008).

Supplementary material for EPAPS

1. Comparison with the positive- P simulations. —

Here, we compare the results of the present treatment using the undepleted molecular approximation and exact first-principles simulations using the positive- P representation [10, 19], in which the molecular depletion is taken into account within the full quantum field theory Hamiltonian. In Fig. 5 we show the corresponding atomic densities for the case of bosonic atoms. Figure 5 (a) is the same one as Fig. 2 (e) of the main text, while Fig. 5 (b) is the corresponding positive- P result. As we see the agreement is very good. First principles simulations for fermionic atoms using the Gaussian stochastic methods of Ref. [20] are still under development, but we expect a similarly good agreement as the molecular depletion is a weaker effect in this case [17, 28].

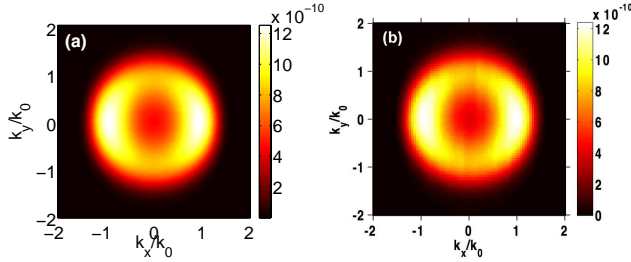


Figure 5: Atomic density in momentum space (in units of m^2) at $t_3/t_0 = 3.3$ within the undepleted molecular field approximation (a) and using the positive- P simulations with molecular depletion (b).

2. Shot noise and relative number variances. — For bosons the uncorrelated shot-noise is determined by Poissonian statistics so that in the case of the smallest counting area we have

$$\begin{aligned} \Delta_{\text{SN}} &= \langle (\Delta \hat{n}_{1,\mathbf{k}_0})^2 \rangle + \langle (\Delta \hat{n}_{2,-\mathbf{k}_0})^2 \rangle \\ &= \langle \hat{n}_{1,\mathbf{k}_0} \rangle + \langle \hat{n}_{2,-\mathbf{k}_0} \rangle. \end{aligned} \quad (8)$$

For fermions, on the other hand, the shot-noise is always sub-Poissonian and is given by [28]

$$\begin{aligned} \Delta_{\text{SN}} &= \langle (\Delta \hat{n}_{1,\mathbf{k}_0})^2 \rangle + \langle (\Delta \hat{n}_{2,-\mathbf{k}_0})^2 \rangle \\ &= \langle \hat{n}_{1,\mathbf{k}_0} \rangle (1 - \langle \hat{n}_{1,\mathbf{k}_0} \rangle) + \langle \hat{n}_{2,-\mathbf{k}_0} \rangle (1 - \langle \hat{n}_{2,-\mathbf{k}_0} \rangle). \end{aligned} \quad (9)$$

The relative number variance can be written in the

following form [10, 19, 29]:

$$V_{\mathbf{k}_0,-\mathbf{k}_0}(t) = \frac{\langle \hat{n}_{1,\mathbf{k}_0} \hat{n}_{1,\mathbf{k}_0} \rangle - \langle \hat{n}_{1,\mathbf{k}_0} \rangle \langle \hat{n}_{2,-\mathbf{k}_0} \rangle}{\Delta_{\text{SN}}}, \quad (10)$$

where we have taken into account that $\langle \hat{n}_{1,\mathbf{k}_0} \rangle = \langle \hat{n}_{2,-\mathbf{k}_0} \rangle \equiv n_{\mathbf{k}_0}$ and $\langle \hat{n}_{1,\mathbf{k}_0} \hat{n}_{1,\mathbf{k}_0} \rangle = \langle \hat{n}_{2,-\mathbf{k}_0} \hat{n}_{2,-\mathbf{k}_0} \rangle$. Note that $\langle \hat{n}_{1,\mathbf{k}_0} \hat{n}_{1,\mathbf{k}_0} \rangle = \langle \hat{n}_{1,\mathbf{k}_0} \rangle = n_{\mathbf{k}_0}$ for fermions. Applying Wick's theorem to calculate the higher-order moments, and introducing the resonant anomalous density $m_{\mathbf{k}_0} \equiv \langle \hat{a}_{1,\mathbf{k}_0} \hat{a}_{2,-\mathbf{k}_0} \rangle$, where $\hat{a}_{j,\mathbf{k}}(t) \equiv \hat{a}_j(\mathbf{k}, t) \sqrt{\Delta k_x \Delta k_y}$ we obtain

$$V_{\mathbf{k}_0,-\mathbf{k}_0}(t) = 1 - \frac{|m_{\mathbf{k}_0}|^2 - n_{\mathbf{k}_0}^2}{n_{\mathbf{k}_0}} \quad (11)$$

for bosons, and

$$V_{\mathbf{k}_0,-\mathbf{k}_0}(t) = 1 - \frac{|m_{\mathbf{k}_0}|^2}{n_{\mathbf{k}_0}(1 - n_{\mathbf{k}_0})}. \quad (12)$$

for fermions. The variance $V_{\mathbf{k}_0,-\mathbf{k}_0}(t)$ is then calculated by numerically solving Eqs. (4) of the main text.

For the case of the largest pair of counting areas, which we refer to as binning, we consider the left (L) and the right (R) halves of the momentum space for bosons, and the bottom (B) and top (T) halves for fermions. Accordingly, we introduce particle number operators $\hat{N}_j^{\text{L(R)}}$ and $\hat{N}_j^{\text{B(T)}}$ ($j = 1, 2$), defined as $\hat{N}_j^{\text{L}} = \sum^{\text{L}} \hat{n}_{j,\mathbf{k}}$ (with a similar convention for R, B, and T), where \sum^{L} and \sum^{R} stand for double sums $\sum^{\text{L}} \equiv \sum_{k_x < 0} \sum_{k_y}$ and $\sum^{\text{R}} \equiv \sum_{k_x > 0} \sum_{k_y}$, whereas $\sum^{\text{B}} \equiv \sum_{k_x} \sum_{k_y < 0}$ and $\sum^{\text{T}} \equiv \sum_{k_x} \sum_{k_y > 0}$. The normalized variance of the relative atom number fluctuations in the spin states 1 and 2 is defined in Eq. (6) of the main text, in which the uncorrelated shot-noise level

$$\Delta_{\text{SN}} = \sum^{\text{R}} \langle (\Delta \hat{n}_{1,\mathbf{k}})^2 \rangle + \sum^{\text{L}} \langle (\Delta \hat{n}_{2,\mathbf{k}})^2 \rangle \quad (13)$$

for bosons is given by

$$\Delta_{\text{SN}} = \sum^{\text{R}} \langle \hat{n}_{1,\mathbf{k}} \rangle + \sum^{\text{L}} \langle \hat{n}_{2,\mathbf{k}} \rangle = \langle \hat{N}_1^{\text{R}} \rangle + \langle \hat{N}_2^{\text{L}} \rangle, \quad (14)$$

while for fermions it is given by

$$\Delta_{\text{SN}} = \sum^{\text{T}} \langle \hat{n}_{1,\mathbf{k}} \rangle (1 - \langle \hat{n}_{1,\mathbf{k}} \rangle) + \sum^{\text{B}} \langle \hat{n}_{2,\mathbf{k}} \rangle (1 - \langle \hat{n}_{2,\mathbf{k}} \rangle), \quad (15)$$

which we note is not same as $[\langle \hat{N}_1^{\text{T}} \rangle (1 - \langle \hat{N}_1^{\text{T}} \rangle) + \langle \hat{N}_2^{\text{B}} \rangle (1 - \langle \hat{N}_2^{\text{B}} \rangle)]$. Applying Wick's theorem to factorize the higher-order moments in Eq. (6) of the main text, we obtain

$$\begin{aligned} V_{\text{LR}}(t) &= \frac{1}{\langle \hat{N}_1^{\text{R}} \rangle} \left[\langle \hat{N}_1^{\text{R}} \rangle \right. \\ &\quad \left. + \sum_{\mathbf{k}}^{\text{R}} \sum_{\mathbf{k}'}^{\text{R}} |\langle \hat{a}_{1,\mathbf{k}}^\dagger \hat{a}_{1,\mathbf{k}'} \rangle|^2 - \sum_{\mathbf{k}}^{\text{R}} \sum_{\mathbf{k}'}^{\text{L}} |\langle \hat{a}_{1,\mathbf{k}} \hat{a}_{2,\mathbf{k}'} \rangle|^2 \right] \end{aligned} \quad (16)$$

for bosons, and

$$V_{\text{BT}}(t) = \frac{1}{\langle \hat{N}_1^{\text{T}} \rangle - \sum_{\mathbf{k}}^{\text{T}} \langle \hat{n}_{1,\mathbf{k}} \rangle^2} \left[\langle \hat{N}_1^{\text{T}} \rangle - \sum_{\mathbf{k}}^{\text{T}} \sum_{\mathbf{k}'}^{\text{T}} |\langle \hat{a}_{1,\mathbf{k}}^\dagger \hat{a}_{1,\mathbf{k}'} \rangle|^2 - \sum_{\mathbf{k}}^{\text{T}} \sum_{\mathbf{k}'}^{\text{B}} |\langle \hat{a}_{1,\mathbf{k}} \hat{a}_{2,\mathbf{k}'} \rangle|^2 \right] \quad (17)$$

for fermions. Here, we have used the fact that $\langle \hat{n}_{1,\mathbf{k}} \rangle = \langle \hat{n}_{1,-\mathbf{k}} \rangle = \langle \hat{n}_{2,\mathbf{k}} \rangle$, $\langle \hat{N}_1^{\text{R}} \rangle = \langle \hat{N}_2^{\text{L}} \rangle$, and $\langle \hat{N}_1^{\text{T}} \rangle = \langle \hat{N}_2^{\text{B}} \rangle$, due to symmetry considerations. The calculation of the variances $V_{\text{LR}}(t)$ and $V_{\text{BT}}(t)$ can now be done using the numerical solution of Eqs. (4) of the main text.